Build-up of Triplet State Population in Operating TQ1:PC71BM Devices Does Not Limit Their Performance

Safakath Karuthedath[1], Julien Gorenflot[1], Armantas Melianas[2†], Zhipeng Kan[1††], Martijn Kemerink[3†††], Frédéric Laquai[1*]*

[1]Materials Science and Engineering Program (MSE), Physical Sciences and Engineering Division (PSE), KAUST Solar Center (KSC), King Abdullah University of Science and Technology (KAUST), Thuwal 23955-6900, Kingdom of Saudi Arabia.

[2]Department of Physics, Chemistry and Biology, Biomolecular and Organic Electronics, Center of Organic Electronics (COE), Linköping University, 58183, Linköping, Sweden.

[3]Complex Materials and Devices, Department of Physics, Chemistry and Biology, Linköping University, 58183, Linköping, Sweden.

AUTHOR INFORMATION

† Present address: Department of Materials Science and Engineering, Stanford University, Stanford, California, 94305, USA.

†† Present address: Organic Semiconductor Research Center, Chongqing Institute of Green and Intelligent Technology, Chinese Academy of Sciences, Chongqing, 400714, China.

[†††] Present address: Centre for Advanced Materials, Ruprecht-Karls-Universität Heidelberg, Heidelberg, D-69120, Germany.

Corresponding Authors

julien.gorenflot@kaust.edu.sa, frederic.laquai@kaust.edu.sa

ABSTRACT

Triplet generation in organic solar cells has been considered a major loss mechanism. Determining the density of the triplet state population in an operating device is challenging. Here, we employ transient absorption (TA) spectroscopy on the quinoxaline–thiophene co-polymer TQ1 blended with $PC_{71}BM$, quantify the transient charge and triplet state densities, and parametrize their generation and recombination dynamics. The charge recombination parameters reproduce the experimentally-measured current-voltage characteristics in charge carrier drift-diffusion simulations, and they yield the steady-state charge densities. We demonstrate that triplets are formed by both geminate and non-geminate recombination of charge carriers and decay primarily by triplet-triplet annihilation. Using the charge densities in the rate equations describing triplet state dynamics, we find that triplet state densities in devices are in the range of charge carrier densities. Despite this substantial triplet state build-up, TQ1:$PC_{71}BM$ devices exhibit only moderate geminate recombination and significantly reduced non-geminate charge recombination, with reduction factors between 10^{-4} to 10^{-3} compared to Langevin recombination.

TOC GRAPHIC

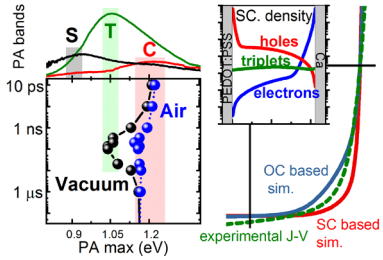

KEYWORDS: organic photovoltaics, triplet states, transient absorption spectroscopy, drift-diffusion simulation, charge carrier dynamics

Organic solar cells (OSC) have demonstrated a steady increase of the power conversion efficiency (PCE) over the past two decades[1-6] thanks to the development of novel materials and a significantly improved understanding of the (photo)physical processes governing device performance, including singlet exciton dissociation, charge carrier recombination, and triplet state formation.[7-17] However, the precise role of triplet states[18] in the physics, performance, and stability of organic solar cells is still debated.

In neat organic films, triplets are formed by intersystem crossing (ISC) from excited singlet states or by singlet fission from higher energy (hot) excitons.[15,19] In donor-acceptor bulk heterojunctions, they are typically created by geminate and/or non-geminate charge recombination, and they are a potential loss channel, whose extent varies from system to system. [8-9, 18, 20-22] However, it is still unclear whether the processes often monitored by pulsed spectroscopy experiments are relevant to steady-state conditions of devices, and at lower (~1 sun) photon flux. Thus, our first objective here is to address this question by determining triplet state densities under solar illumination in operating devices.

Secondly, contradictory reports exist regarding the impact of triplets on device performance. Since they result from charge recombination, triplet formation is sometimes considered a loss channel competing with charge separation or extraction, together with recombination to the ground state.[15, 23, 24] For example, Vardeny's group demonstrated significantly improved photocurrents in PTB7:$PC_{61}BM$ based devices when reducing polymer triplet formation by addition of a spin half-

radical such as galvinoxyl.[25, 26] On the other hand, Chow et al. showed that the encounter of separated charges in polymer:fullerene blends creates CT states of both singlet and triplet spin states (denoted as ^{1}CT and ^{3}CT), which improves the photovoltaic performance due to their ability to re-dissociate into free charge carriers.[8] Moreover, studies by Gehrig et al. demonstrated that when triplets are formed on the polymer, they are a reservoir of excitations, that, to a certain extent, can replenish the charge carrier population via triplet-triplet annihilation in PBDTTC-C:$PC_{61}BM$ blends.[18]

For the present study, we chose blends of the donor polymer TQ1 and fullerene derivative $PC_{71}BM$, since they exhibit clear triplet formation,[27] yet they also exhibit high internal quantum efficiencies in devices.[28-31] We observed, quantified, and parametrized both charge and triplet state formation and decay, which in turn enabled us, not only to simulate charge densities in operating devices, but also to calculate the corresponding triplet densities by solving the triplet rate equation under steady-state conditions. More precisely, the kinetics of charges and triplets were acquired by transient absorption (TA) spectroscopy combined with multivariate curve resolution - alternating least square (MCR-ALS) data analysis. The corresponding triplet and charge densities were obtained by determining the triplet and charge absorption cross-section. The charge decay was parametrized using a two-pool charge recombination model, while different rate equations were tested to fit the triplet dynamics. Charge recombination parameters were used to simulate the bias dependence of the photocurrent in devices under steady-state conditons, and were found to reproduce the experimentally-measured current-voltage characteristics very well, confirming the relevance of parameters determined by transient spectroscopy to steady-state photophysics, and providing the charge densities under device operating conditions. The charge densities enabled us to determine the triplet densities in operating devices. Interestingly, we find that the triplet density

can be as high as half the charge carrier density under short circuit condition; yet, this does not impede charge separation and extraction.

The chemical structures of the donor polymer TQ1 (poly[2,3-bis(3-octyloxyphenyl)quinoxaline-5,8-diyl-alt-thiophene-2,5-diyl]) and the fullerene acceptor PC71BM are shown in Figure 1a. Figure 1b shows the steady-state absorption spectra of pristine and blend films. Current-voltage characteristics (J-V), external quantum efficiency (EQE), and internal quantum efficiency (IQE) spectra are shown in panel c and d, respectively. The devices based on TQ1:$PC_{71}BM$ (1:2.5 wt %) used in this study reached a power conversion efficiency of 6%, which is well in line with previously reported values.[28, 32] The rather high IQE (average around 82%) and fill factor (63-65%) indicate that the device efficiency is limited primarily by insufficient light absorption, while charge extraction dominates over non-geminate recombination, even at low internal fields.

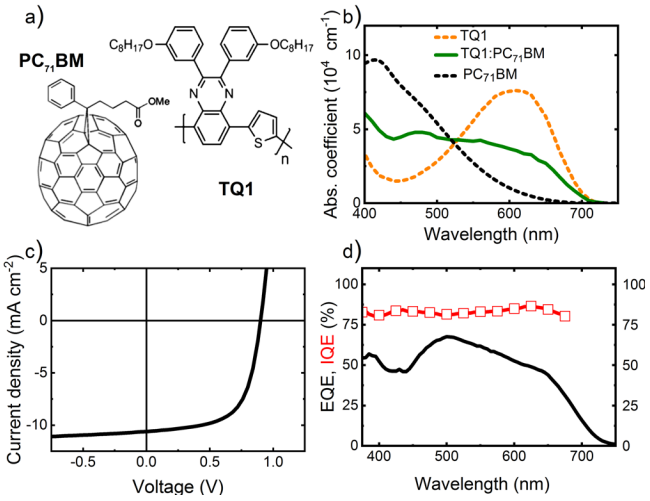

Figure 1. (a) Chemical structure of the donor polymer TQ1 and fullerene acceptor $PC_{71}BM$. **(b)** Absorption coefficients of neat TQ1 and $PC_{71}BM$ films (dashed lines) and TQ1:$PC_{71}BM$ thin film blend (solid line) **(c)** Current-voltage characteristics of a photovoltaic device with TQ1:$PC_{71}BM$

as photoactive layer measured under AM1.5G illumination. **(d)** EQE (black line) and IQE (open red squares and solid line) spectra of the TQ1:$PC_{71}BM$ device.

We used transient absorption (TA) spectroscopy to monitor the excited state dynamics from sub-ps to microseconds.[33-35] Furthermore, we used MCR-ALS to separate the individual spectra and dynamics of the excited states contributing to the total TA signal.[36-39] MCR-ALS is a soft modeling tool introduced earlier by Tauler et al. and previously used by us and others to analyze TA data.[36-38, 40] More details about MCR-ALS can be found elsewhere.[18, 19, 40-43]

The signatures of TQ1 singlets (broad photoinduced absorption, PA, peaking at 0.9 eV) and triplets (broad PA peaking at 1 eV) are first identified in neat TQ1 films by picosecond-nanosecond (ps-ns) TA spectroscopy (Figure S1). The same triplet feature is obtained upon triplet sensitization of TQ1 films using platinum porphyrin (PtOEP) as dopant. Singlet and triplet state dynamics, separated by MCR-ALS, show that in neat TQ1 films triplets are formed by intersystem crossing from singlet excitons with some second order contribution from singlet-singlet annihilation at high fluences (see Figure S1).

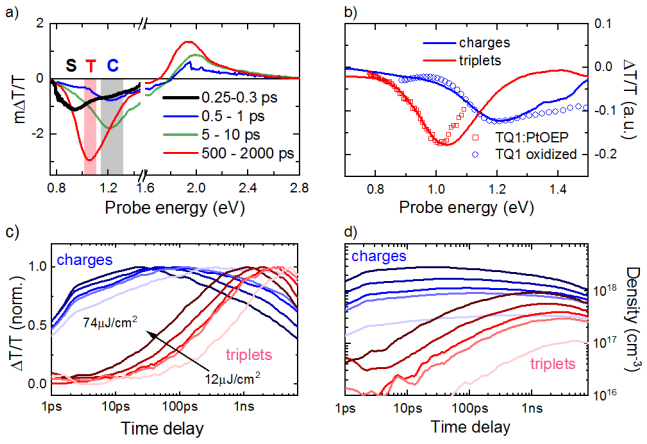

Figure 2. (a) ps-ns TA spectra of TQ1:$PC_{71}BM$ blend films measured in vacuum after excitation at 500 nm. **(b)** MCR-ALS component spectra assigned to triplet states (red line) and charges (blue

line) in TQ1:$PC_{71}BM$. The open symbols denote experimentally measured triplet (red square) and charge (blue circles) induced absorption spectra obtained from PtOEP-doped TQ1 films and iron (III) chloride-oxidized TQ1 films, respectively. **(c)** Corresponding (normalized) kinetics of triplets (red shades) and charges (blue shades) obtained from MCR-ALS for a range of pump fluences. **(d)** Corresponding population density transients calculated by using the excited-state cross-sections.

TQ1 singlet and TQ1 triplet excitons are also found in the ps-ns transient absorption spectra of TQ1:$PC_{71}BM$ blend films, see Figure 2a, at sub-picosecond (black spectrum), and nanosecond (red spectrum) timescales, respectively. Charges dominate the spectra at ps times (blue and green TA spectra), with a PA peaking at 1.2 eV corresponding to the absorption observed for oxidized TQ1 (cation) films (see Figure 2c). The rise of the charge-induced absorption signal (tens to hundreds of ps) is delayed compared to the TQ1 exciton-induced decay (sub-picoseconds), which we attribute to the diffusion of excitons in fullerene-rich domains. Triplet formation is accompanied by a substantial rise of the signal amplitude, and quenched in the presence of oxygen (Figure S4).

Triplet and charge kinetics can be monitored at their respective PA peaks (Figure S3b), but are separated here by MCR-ALS (Figure 2b-d). Triplet formation accelerates with fluence, indicating a higher order process such as non-geminate recombination is involved in triplet formation, in line with earlier reports on similar fullerene-based material systems.[9, 18, 20, 44, 45]

Charge and triplet state transients are converted into transient excited state densities using their respective absorption cross-sections; singlets: $1.6\pm0.1\times10^{-16}$ cm^2 (at 0.93 eV), triplets: $3\pm0.3\times10^{-16}$ cm^2 (at 1.02 eV), and charges: $0.8\pm.08\times10^{-16}$ cm^2 (at 1.2 eV), respectively. Singlet and triplet cross-sections were determined on neat TQ1 films using the absorbed photon density for singlets and assuming that singlets and triplets exhibit the same photobleach (details can be found in the

S.I. and Figure S9). The charge carrier cross-section was determined from blends assuming that at low fluence each absorbed photon is converted into a charge, in line with the high device IQE (*vide infra*). We note that the absorption cross-section of charge carriers determined here is in line with a previous report.[46] The much larger cross-section of triplets compared to charges explains well the signal rise observed upon triplet generation by charge recombination. For all fluences, the triplet density reaches approximately 21% of the maximum charge density. However, the peak of the population is reached at later times for lower fluences. Thus, it remains unclear, whether triplets are formed in devices at low fluence, and if charges can be extracted prior to the reaching the peak of the triplet density. We parametrized the rates governing charge and triplet densities and used nanosecond to microsecond TA, when most of the triplet formation and decay occur.

ns-µs TA confirms the triplet formation in the nanosecond time scale, indicated by the PA red shift and signal rise, see Figure 3a, extending up to several ns at the lowest fluences. However, strikingly this trend reverts on the ns-µs timescale (see Figure 3b).[31] Again, these transient evolutions are quenched in air (Figure 3b), confirming the assignment to triplet formation and decay.

MCR-ALS decomposition also reveals that triplets undergo a fast rise followed by a fast decay (Figure 3e), while charges exhibit a monotonous and slower decay (Figure 3c). The component-associated spectra can be found in Figure S5a. The MCR-ALS spectral components are virtually identical to those obtained by MCR-ALS of the ps-ns TA data. The fast decay of the triplets leaves the charges as the main excited state population on the hundreds of ns to µs time scale, thereby explaining the observed blue-shift of the TA signal. The time-scale of the triplet density decay and its strong fluence dependence (Figure 3e) point to bimolecular processes such as triplet-triplet annihilation or triplet-charge annihilation rather than triplet state recombination to the ground state.

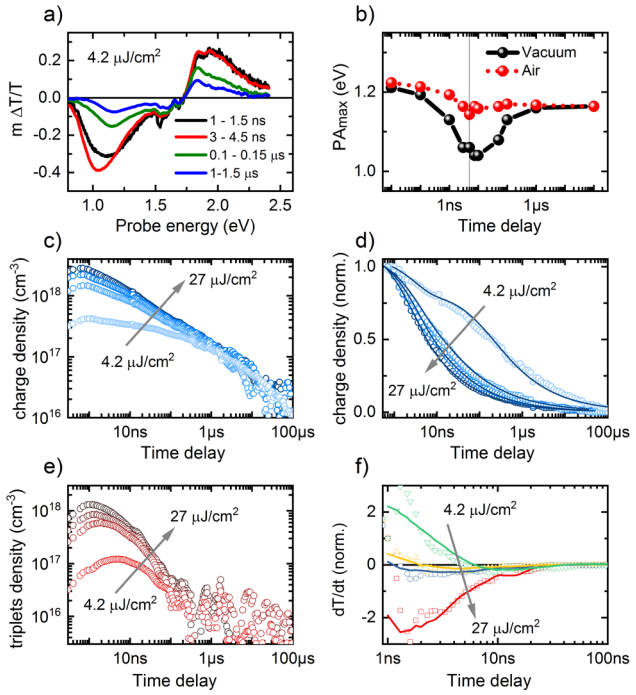

Figure 3. Charge carrier and TQ1 triplet state formation and decay on the ns-µs timescale and their parametrization. **(a)** ns-µs TA spectra of TQ1:PC71BM blend after excitation at 532 nm. **(b)** Shift of the maximum of the photoinduced absorption with time in vacuum (black line with symbols), indicating triplet formation followed by their decay, as well as in air (dotted red line with symbols), indicating triplet quenching. **(c)** Transient charge carrier density extracted by MCR-ALS and (d) global fit to a two-pool charge recombination model. **(e)** Transient TQ1 triplet density as extracted from MCR-ALS and (f) fit of the variation of the triplet state density considering formation by charge recombination and decay by triplet-triplet annihilation (Equation (1)).

In order to determine the charge and triplet state density under device operating conditions, we extracted the kinetic parameters from the ns-µs transients and used them in carrier drift-diffusion steady-state device photocurrent simulations.

Precisely, we parametrized the charge dynamics using a semi-empirical two-pool charge carrier recombination model.[33, 47] In that model, geminate recombination is parametrized by the fraction *1-f* of charges that fail to separate and thus undergo geminate recombination, and by the geminate charge pair lifetime, $\tau_{CT} = 1/k_{CT\rightarrow GS}$, with $k_{CT\rightarrow GS}$ the geminate recombination rate. Non-geminate recombination is parametrized by the fraction *f* of separated charges, the recombination coefficient γ, and the apparent recombination order $\lambda+1$, which describes the empirically observed non-geminate recombination of separated charges (n_{sc}) rate of $R = \gamma\, n_{sc}^{\lambda+1}$ (corresponding to a power-law decay with a power of $-1/\lambda$ in transient measurements). The parameters were extracted by global fits to the charge carrier decays measured at four different excitation fluences (see Figure 3d), allowing only the initial charge densities n_0 to vary between fluences.

Table 1 - Parameters obtained by fitting the ns-µs charge carrier recombination dynamics in TQ1:$PC_{71}BM$ blends to a two-pool charge recombination model.

f	τ_{CT} $= 1/k_{CT\rightarrow GS}$	$\lambda + 1$	γ $(cm^3)^{\lambda}s^{-1}$	k_2 (cm^3s^{-1})	$k_{2,TDCF}$ (cm^3s^{-1})
0.82	2.8 ns	3.2	1.13×10^{-32}	7.2×10^{-14} (sc) 1.5×10^{-12} (oc)	2.3×10^{-11}

$k_{2,TA}$ is the bimolecular recombination coefficient that would yield the same rate as the empirical high order recombination ($k_{2,TA}n^2 = \gamma\, n^{\lambda+1}$ so $k_{2,TA} = \gamma\, n^{\lambda-1}$) for a carrier density $n = 5.0\times10^{15}$ cm^{-3}, corresponding to a device in short circuit (sc) conditions under 1 sun illumination as obtained from steady-state device simulation and $n = 6.2\times10^{16}$ cm^{-3}, corresponding to a device in open circuit (oc) conditions under 1 sun illumination as obtained from steady state device simulation (*vide infra*). $k_{2,TDCF}$ is shown for comparison; it is the bimolecular recombination coefficient obtained from a fit of the transient Time Delayed Collection Field measurements however, neglecting recombination with dark (injected) carriers (see Figure S12).

The extracted parameters are summarized in Table 1. Two important observations have been made: first, a rather efficient charge separation (f = 82 %) that matches the experimentally-determined IQE, see Figure 1d, suggesting that incomplete charge separation is the only loss at short circuit (other than the incomplete photon absorption). Second, a very high apparent non-geminate recombination order $\lambda+1$, indicating a super-linear dependence of the bimolecular recombination coefficient on the carrier concentration n. This implies that non-geminate recombination losses are considerably reduced at the low fluences of solar cell operating conditions.

Next, we parametrized the rise of the triplet population and decay. We note that, while the rate equations used in the two-pool charge recombination model have an analytical solution, equivalent models that describe the triplet state density do not. Therefore, we directly fit the rates, that is, the time-derivative of the triplet state density, instead of the transient density itself. Again, we used the same set of parameters to globally fit the rates at different excitation densities, varying only the initial rates dT_0/dt of each fluence.

For the triplet formation, we considered two possibilities: free charge recombination only, and both geminate and non-geminate recombination. For the triplet state decay, we considered triplet recombination to the ground state, triplet-charge annihilation, and triplet-triplet annihilation. However, the best fit was obtained for triplet state generation by both geminate and non-geminate charge recombination and triplet state decay via triplet-triplet annihilation. Indeed non-geminate recombination alone does not describe the triplet generation at low fluences, where the triplet density increases, while non-geminate recombination is still negligible. Similarly, triplet-charge annihilation is insufficient to reproduce the strong fluence dependence of triplet density decay. However, we cannot entirely rule out that triplet-charge annihilation occurs as well, yet adding it did not improve the fit and thus we did not consider it further to avoid over-parametrization. We

note that triplet–charge annihilation has an even lesser impact in devices, where charges are extracted. As a result, we found the triplet state population dynamics are best described by the following rate equation:

$$\frac{dT}{dt} = \alpha R - k_{TT} T^2 \quad (1)$$

Where T represents the triplet density, R is the charge carrier recombination rate (obtained for the fit by derivation of the parametrized charge density decay), α is the triplet formation efficiency, and k_{TT} the rate coefficient for triplet-triplet annihilation. The best fit is shown in Figure 3f, the fits for other models can be found in Figure S13. The fit yielded values of α = 0.94 ± 0.03 and k_{TT} = (3.9 ± 0.2) × 10^{-10} cm^3s^{-1}. We note however, that the error bars do not take into account the incertitude of the absorption cross-section (specifically of triplets) and suggest considering the order of magnitude rather than the absolute values obtained here. In particular this could explain why we obtain a value of α larger than 0.75, which is unexpected in view of spin statistics. On the other hand, we cannot exclude that the lower coupling of spins at the interface and the energy difference between ^{3}CT and ^{1}CT could lead to spin-flip and the formation of more than 75% of ^{3}CT prior to their transfer to the TQ1 triplets that we monitor in TA.

We used 1D charge carrier drift-diffusion simulations combined with optical modeling (Setfos 4.6 from Fluxim) to simulate the current-voltage characteristics of operating TQ1:$PC_{71}BM$ solar cells under illumination equivalent to 1 sun. The impact of geminate recombination was taken into account by using f, the fraction of charges undergoing non-geminate recombination from TA as the charge generation efficiency. We note that f was found to be equal to the IQE thus, no additional loss is considered prior to charge transfer. Non-geminate recombination parameters are used to compute the reduction factor ζ compared to Langevin recombination. Details as well as other

parameters can be found in the S.I. Due to the strong *n*-dependence of non-geminate recombination, we computed two boundary values for ζ: at low charge densities obtained upon significant extraction at short circuit and at higher charge density obtained in the absence of carrier extraction, *i.e.*, at open circuit condition. Furthermore, we calculated the reduction factor based on the bimolecular recombination factor extracted from time-delayed collection field measurements, see also Figure S12.

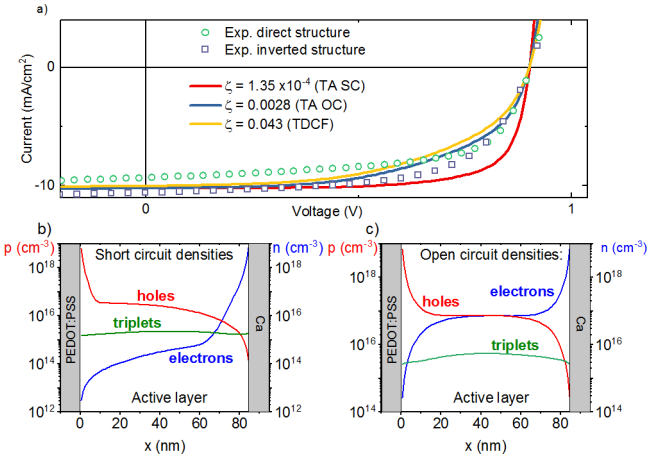

Figure 4. Setfos simulation reproduces experimental JV curves and enables to determine steady-state excited state densities. **(a)** J-V curves measured (symbols) and simulated (solid lines) considering different non-geminate recombination rates: TA SC indicates the simulated J-V curve based on the recombination reduction factor (ζ) estimated from TA using the *n*-dependent non-geminate recombination rates and short circuit charge density, TA OC from TA rate and open circuit charge density, and TDCF represents the J-V curve simulated by using ζ obtained from TDCF experiments. **(b)** Simulated charge densities under short circuit condition as well as corresponding triplet densities computed using equation (1). **(c)** Simulated charge densities under open circuit condition as well as corresponding triplet densities computed using equation (1).

Figure 4 shows the two boundary cases of ζ calculated for open circuit and short circuit conditions, respectively. As expected, computing ζ from carrier densities at open circuit leads to overestimated recombination (lower *ff)*, while using densities at short circuit, ζ underestimates recombination (higher *ff*). However, the agreement with experimental data is still reasonable in both cases. Notably, using recombination based on $k_{2,TDCF}$ leads to a larger overestimation of recombination in the low carrier extraction regime (i.e. close to V_{OC}), in turn leading to a lower photocurrent and fill factor. This is most likely caused by underestimation of the charge carrier density in TDCF experiments (where we neglected dark (injected) carriers), leading to an overestimated recombination coefficient (see Figure S12 and further discussion in the S.I.).[48]

With the steady-state charge densities at hand, we calculated the corresponding recombination rates: $R = R_{CT} + k_{\lambda}n^{\lambda+1}$, where R_{CT} is the rate of recombination of bound pairs (at equilibrium $R_{CT} = (1-f)G$, where G is the rate of excited state generation) and used them in Equation (1) under steady-state condition (that is, $dT/dt = 0$) to extract the steady-state triplet density. The densities together with the other simulation parameters are reported in Table 2. As can be seen, we find triplet densities in devices ranging from close to 10% of the charge density at open circuit conditions, up to half of the charge density upon short circuit conditions. Importantly, as depicted in figure 4b, the triplet density under short circuit conditions is larger than the density of electrons in most of the photoactive layer.

Table 2 – Figures of merit obtained from experiments and simulations of TQ1:$PC_{71}BM$ based solar cells.

Device structure and conditions used in simulations of JV curves	$n^{(a)}$ cm^{-3}	k_2 $cm^3 \cdot s^{-1}$	$\zeta = k_2/k_{Langevin}$	T cm^{-3}	PCE %	J_{SC} $mA.cm^{-2}$	FF %	V_{OC} V

Experimental result (inverted structure) [(b)]	N/A	N/A	N/A	N/A	7.0 [1]	- 10.6	63	0.9
Experimental result (direct structure) [(c)]	N/A	N/A	N/A	N/A	5.75	- 9.9	65	0.9
Simulated device [(c)] using $k_{2,TDCF}$	N/A	2.3×10^{-11}	4.3×10^{-2}	N/A	4.56	- 9.8	51	0.9
Simulated device [(c)] using $k_{2,TA}$ $(n = n_{oc})$	$n_{oc} = 6.2\times10^{16}$	1.5×10^{-12}	2.8×10^{-3}	5.3×10^{15}	5.22	- 10.1	57	0.9
Simulated device using $k_{2,TA}$ $(n = n_{sc})$ [(c)]	$n_{sc} = 5.0\times10^{15}$	7.2×10^{-14}	1.35×10^{-4}	2.5×10^{15}	6.57	- 10.2	72	0.9

(a) Charge density used to evaluate $k_2 = k_\lambda n^{\lambda-1}$, and hence ζ in the simulation. (b) Inverted device structure: Glass/Al/TiOx/TQ1:$PC_{71}BM$/PEDOT:PSS with thicknesses in nanometers: -/80/2/70-80/120 (c) direct device structure: Glass/ITO/PEDOT:PSS/TQ1:$PC_{71}BM$/Ca/Al with thicknesses in nanometers: -/109/40/80-90/5/80 (active layer: 85 nm in the simulation).

Overall, we see that TQ1:$PC_{71}BM$ devices exhibit minimal losses and high steady-state triplet densities. Specifically, geminate recombination losses are moderate (18%) and are the only loss (apart from the incomplete photon absorption) under short circuit conditions. Non-geminate recombination rates are extremely low with prefactors between 7.2×10^{-14} $cm^{-3}s^{-1}$ and 1.5×10^{-12} $cm^{-3}s^{-1}$, *i.e.*, at the very low end of values typically reported for OPV.[32, 33, 46, 49] This in turn leads to high fill factors, especially when considering the low hole mobility of only around 10^{-5} $cm^2V^{-1}s^{-1}$, that could in principle lead to strong recombination due to space charge accumulation.

The good performance, despite the large triplet densities observed in the device, indicates the existence of a charge recombination channel that is generating triplets very efficiently (94% yield), yet is not necessarily detrimental to device performance. On the contrary, the same donor blended with the acceptor polymer N2200 exhibits no triplet formation, but large recombination losses, causing a low fill factor, while the two blends have no significant morphological differences. [50]

However, the question whether the high triplet density causes the strongly reduced non-geminate recombination remains open. Triplet states may serve as a reservoir of excitations, as they can recreate charges via triplet-triplet annihilation (the main triplet density decay mechanism in TQ1:$PC_{71}BM$), thereby delaying the decay of the charge density. Indeed, charge formation upon triplet-triplet annihilation (TTA) has been reported in other organic bulk heterojunctions.[12] Moreover, that triplet states can be a reservoir of excitations in organic semiconductors is an established fact employed in applications such as thermally-stimulated delayed fluorescence.[51-53]

In summary, we used TQ1:$PC_{71}BM$ as a model system to investigate the presence of triplet states and their impact on the performance of operating OSCs. TQ1:$PC_{71}BM$ as active layer exhibits efficient exciton-to-charge conversion (IQE of 82%) even at low internal fields (fill factor of 63-64 %), while (transient) excited state spectroscopy showed significant triplet formation. Transient absorption spectroscopy performed on TQ1:$PC_{71}BM$ films revealed nanosecond, strongly fluence-dependent triplet formation and decay. Triplet and charge carrier dynamics were separated by MCR-ALS and the corresponding densities were quantified using estimates of their absorption cross-sections. Charge and triplet fluence-dependent kinetics were modeled and parametrized, revealing that in pulsed laser experiments, both geminate and non-geminate recombination of charge carriers result in very efficient formation of triplet states. Non-geminate recombination however, was found to be strongly carrier concentration dependent, and thus occurs mainly at higher charge densities than those present in operating devices. Using the extracted kinetic parameters in steady-state device photocurrent simulations confirmed that non-geminate recombination is much reduced under solar illumination conditions, with reduction factors in the range of 10^{-4} – 10^{-3}. However, 18% of the photogenerated charge carriers fail to separate and thus recombine geminately, resulting in the formation of triplet states. Triplet states are long-lived in

the blend and can accumulate to densities of around half the free charge carrier density under short circuit conditions, their density only limited by triplet-triplet annihilation. The high triplet densities coupled with very low charge recombination losses indicate that triplet states do not necessarily reduce the performance of organic solar cells, in contrast to previous conclusions.[9,55] We stress that triplet formation is a very common feature in OPV blends,[7-31] and that given their possibly large equilibrium density, it seems important to consider their impact on performance. The approach presented here is fairly universal and enhances our understanding of the role of triplet states in increasing or reducing carrier recombination losses.

EXPERIMENTAL METHODS

J-V curves were recorded with a Keithley 2400 Source Meter under AM 1.5G illumination (100 mW cm-2), generated by a solar simulator with a 180 Watt xenon arc lamp as the light source (Model SS50A, Photo Emission Tech., Inc.). Light intensity was set to 1 sun intensity using a standard silicon photodiode calibrated at the Energy Research Centre of the Netherlands (ECN). EQE spectra were recorded with a home-built setup using a Newport Merlin lock-in amplifier. Devices were illuminated with chopped monochromatic light through the transparent ITO electrode. Measured EQE spectra were scaled so that the estimated short-circuit current density from the EQE measurement matched the short-circuit current density of the corresponding JV curve. Details of IQE calculations can be found in Ref.[54]

TA spectroscopy was carried out using a homebuilt pump–probe setup. Two different configurations of the setup were used for either short delay, namely 100 fs to 8 ns experiments, or long delay, namely 1 ns to 300 μs delays, as described below:

The output of a titanium:sapphire amplifier (Coherent LEGEND DUO, 4.5 mJ, 3 kHz, 100 fs) was split into two beams (2 and 1.5 mJ). A fraction of the remaining 1.5 mJ output beam of the LEGEND DUO was focused into a c-cut 3 mm thick sapphire window, thereby generating a white-light supercontinuum from 500 to 1600 nm. The 2 mJ/pulse beam was used to separately pump an optical parametric amplifiers (OPA) (Light Conversion TOPAS Prime) to generate tunable pump pulses. The probe pathway length to the sample was kept constant at ≈5 m between the output of LEGEND and the sample while the pump pathway length was varied between 5.12 and 2.6 m with a broadband retroreflector mounted on an automated mechanical delay stage (Newport linear stage IMS600CCHA controlled by a Newport XPS motion controller), thereby generating delays between pump and probe from −400 ps to 8 ns.

For the 1 ns to 300 μs delay (long delay) TA measurement, the same probe white-light supercontinuum was used as for the 100 fs to 8 ns delays. Here the excitation light (pump pulse) was provided by an actively Q-switched Nd:YVO4 laser (InnoLas picolo AOT) frequency-doubled to provide pulses at 532 nm. The pump laser was triggered by an electronic delay generator (Stanford Research Systems DG535) itself triggered by the transistor– transistor logic (TTL) sync from the Legend DUO, allowing control of the delay between pump and probe with a jitter of roughly 100 ps.

Pump and probe beams were focused on the sample which was kept under a dynamic vacuum of $<10^{-5}$ mbar. The transmitted fraction of the white light was guided to a custom-made prism spectrograph (Entwicklungsbüro Stresing) where it was dispersed by a prism onto a 512 pixel complementary metal-oxide semiconductor (CMOS) linear image sensor (Hamamatsu G11608-512DA). The probe pulse repetition rate was 3 kHz, while the excitation pulses were mechanically chopped to 1.5 kHz (100 fs to 8 ns delays) or directly generated at 1.5 kHz frequency (1 ns to 300

μs delays), while the detector array was read out at 3 kHz. Adjacent diode readings corresponding to the transmission of the sample after excitation and in the absence of an excitation pulse were used to calculate ΔT/T. Measurements were averaged over several thousand shots to obtain a good signal-to noise ratio. The chirp induced by the transmissive optics was corrected with a homebuilt Matlab code. The delay at which pump and probe arrive simultaneously on the sample (i.e., zero time) was determined from the point of maximum positive slope of the TA signal rise for each wavelength.

ASSOCIATED CONTENT

Supporting Information. Complementary TA spectra (pristine material, different fluences on the blends); details of the determination of absorption cross-sections; determination of the effective bimolecular recombination coefficient; time-delayed collection field; fits of alternative rate equations to triplet density rate dynamics; details and explanation of the parameter used for device simulation, and finally steady-state density calculation details are available free of charge in the Supporting Information.

AUTHOR INFORMATION

Notes

S. K and J. G equally contributed to this work. The authors declare no competing financial interest.

Corresponding Authors

*E-mail: julien.gorenflot@kaust.edu.sa, frederic.laquai@kaust.edu.sa

ORCID

Karuthedath S.: 0000-0001-7568-2825

Gorenflot J.: 0000-0002-0533-3205

Melianas A.: 0000-0002-3443-0987

Kan Z.: 0000-0003-1378-541X

Kemerink M.: 0000-0002-7104-7127

Laquai F.: 0000-0002-5887-6158

URL

UltraFast Dynamics group, KAUST Solar Center: https://ufd.kaust.edu.sa/Pages/Home.aspx

ACKNOWLEDGMENT

This publication is based upon work supported by the King Abdullah University of Science and Technology (KAUST) Office of Sponsored Research (OSR) under Award No: OSR-2018-CARF/CCF-3079. The authors thank Dr. Fabian Etzold for the reference spectra of triplets and charges in TQ1. A.M. gratefully acknowledges support from the Knut and Alice Wallenberg Foundation (KAW 2016.0494) for Postdoctoral Research at Stanford University.

REFERENCES

(1) Deibel, C.; Dyakonov, V., Polymer–Fullerene Bulk Heterojunction Solar Cells. *Rep. Prog. Phys.* **2010**, *73* (9), 096401.

(2) Günes, S.; Neugebauer, H.; Sariciftci, N. S., Conjugated Polymer-Based Organic Solar Cells. *Chem. Rev.* **2007**, *107* (4), 1324-1338.

(3) He, Z.; Xiao, B.; Liu, F.; Wu, H.; Yang, Y.; Xiao, S.; Wang, C.; Russell, T. P.; Cao, Y., Single-junction Polymer Solar Cells with High Efficiency and Photovoltage. *Nature Photon.* **2015**, *9* (3), 174-179.

(4) Inganäs, O., Organic Photovoltaics Over Three Decades. *Adv. Mater.* **2018**, *30* (35), 1800388.

(5) Meng, L.; Zhang, Y.; Wan, X.; Li, C.; Zhang, X.; Wang, Y.; Ke, X.; Xiao, Z.; Ding, L.; Xia, R. et al., Organic and Solution-processed Tandem Solar Cells with 17.3% Efficiency. *Science* **2018**, *361* (6407), 1094-1098.

(6) Thompson, B. C.; Fréchet, J. M. J., Polymer–Fullerene Composite Solar Cells. *Angew. Chem. Int. Ed.* **2008**, *47* (1), 58-77.

(7) Dimitrov, S. D.; Wheeler, S.; Niedzialek, D.; Schroeder, B. C.; Utzat, H.; Frost, J. M.; Yao, J.; Gillett, A.; Tuladhar, P. S.; McCulloch, I. et al., Polaron Pair Mediated Triplet Generation in Polymer/Fullerene Blends. *Nat. Commun.* **2015**, *6*, 6501.

(8) Chow, P. C. Y.; Gélinas, S.; Rao, A.; Friend, R. H., Quantitative Bimolecular Recombination in Organic Photovoltaics through Triplet Exciton Formation. *J. Am. Chem. Soc.* **2014**, *136* (9), 3424-3429.

(9) Rao, A.; Chow, P. C. Y.; Gelinas, S.; Schlenker, C. W.; Li, C.-Z.; Yip, H.-L.; Jen, A. K. Y.; Ginger, D. S.; Friend, R. H., The Role of Spin in the Kinetic Control of Recombination in Organic Photovoltaics. *Nature* **2013**, *500* (7463), 435-439.

(10) Howard, I. A.; Etzold, F.; Laquai, F.; Kemerink, M., Nonequilibrium Charge Dynamics in Organic Solar Cells. *Adv. Energy Mater.* **2014**, *4* (9), 1301743.

(11) Albrecht, S.; Schindler, W.; Kurpiers, J.; Kniepert, J.; Blakesley, J. C.; Dumsch, I.; Allard, S.; Fostiropoulos, K.; Scherf, U.; Neher, D., On the Field Dependence of Free Charge Carrier Generation and Recombination in Blends of PCPDTBT/PC70BM: Influence of Solvent Additives. *J. Phys. Chem. Lett.* **2012**, *3* (5), 640-645.

(12) Melianas, A.; Pranculis, V.; Xia, Y.; Felekidis, N.; Inganäs, O.; Gulbinas, V.; Kemerink, M., Photogenerated Carrier Mobility Significantly Exceeds Injected Carrier Mobility in Organic Solar Cells. *Adv. Energy Mater.* **2017**, *7* (9), 1602143.

(13) Jin, F.; Ding, G.; Wang, Y.; Yuan, J.; Guo, W.; Yuan, H.; Sheng, C.; Ma, W.; Zhao, H., Thermal Annealing Effect on Ultrafast Charge Transfer in All-Polymer Solar Cells with a Non-Fullerene Acceptor N2200. *J. Phys. Chem. C* **2017**, *121* (16), 8804-8811.

(14) Löslein, H.; Ameri, T.; Matt, G. J.; Koppe, M.; Egelhaaf, H. J.; Troeger, A.; Sgobba, V.; Guldi, D. M.; Brabec, C. J., Transient Absorption Spectroscopy Studies on Polythiophene–Fullerene Bulk Heterojunction Organic Blend Films Sensitized with a Low-Bandgap Polymer. *Macromol. Rapid Commun.* **2013**, *34* (13), 1090-1097.

(15) Dyer-Smith, C.; Reynolds, L. X.; Bruno, A.; Bradley, D. D. C.; Haque, S. A.; Nelson, J., Triplet Formation in Fullerene Multi-Adduct Blends for Organic Solar Cells and Its Influence on Device Performance. *Adv. Funct. Mater.* **2010**, *20* (16), 2701-2708.

(16) Devižis, A.; Serbenta, A.; Meerholz, K.; Hertel, D.; Gulbinas, V., Ultrafast Dynamics of Carrier Mobility in a Conjugated Polymer Probed at Molecular and Microscopic Length Scales. *Phys. Rev. Lett.* **2009**, *103* (2), 027404.

(17) Ramirez, I.; Causa', M.; Zhong, Y.; Banerji, N.; Riede, M., Key Tradeoffs Limiting the Performance of Organic Photovoltaics. *Adv. Energy Mater.* **2018**, *8* (28), 1703551.

(18) Gehrig, D. W.; Howard, I. A.; Laquai, F., Charge Carrier Generation Followed by Triplet State Formation, Annihilation, and Carrier Recreation in PBDTTT-C/PC60BM Photovoltaic Blends. *J. Phys. Chem. C* **2015**, *119* (24), 13509-13515.

(19) Ochsmann, J. R.; Chandran, D.; Gehrig, D. W.; Anwar, H.; Madathil, P. K.; Lee, K.-S.; Laquai, F., Triplet State Formation in Photovoltaic Blends of DPP-Type Copolymers and PC71BM. *Macromol. Rapid Commun.* **2015**, *36* (11), 1122-1128.

(20) Etzold, F.; Howard, I. A.; Forler, N.; Melnyk, A.; Andrienko, D.; Hansen, M. R.; Laquai, F., Sub-ns Triplet State Formation by Non-geminate Recombination in PSBTBT:PC70BM and PCPDTBT:PC60BM Organic Solar Cells. *Energy Environ. Sci.* **2015**, *8* (5), 1511-1522.

(21) Di Nuzzo, D.; Aguirre, A.; Shahid, M.; Gevaerts, V. S.; Meskers, S. C. J.; Janssen, R. A. J., Improved Film Morphology Reduces Charge Carrier Recombination into the Triplet Excited State in a Small Bandgap Polymer-Fullerene Photovoltaic Cell. *Adv. Mater.* **2010**, *22* (38), 4321-4324.

(22) Etzold, F; Howard, I. A; Mauer, R.; Meister, M.; Kim, T-D.; Lee, K-S.; Baek, N. S.; Laquai, F., Ultrafast Exciton Dissociation Followed by Nongeminate Charge Recombination in PCDTBT:PCBM Photovoltaic Blends. *J. Am. Chem. Soc.* **2011**, *133*(24), 9469-9479

(23) Veldman, D.; Meskers, S. C. J.; Janssen, R. A. J., The Energy of Charge-Transfer States in Electron Donor–Acceptor Blends: Insight into the Energy Losses in Organic Solar Cells. *Adv. Funct. Mater.* **2009**, *19* (12), 1939-1948.

(24) Westenhoff, S.; Howard, I. A.; Hodgkiss, J. M.; Kirov, K. R.; Bronstein, H. A.; Williams, C. K.; Greenham, N. C.; Friend, R. H., Charge Recombination in Organic Photovoltaic Devices with High Open-Circuit Voltages. *J. Am. Chem. Soc.* **2008**, *130* (41), 13653-13658.

(25) Basel, T.; Huynh, U.; Zheng, T.; Xu, T.; Yu, L.; Vardeny, Z. V., Optical, Electrical, and Magnetic Studies of Organic Solar Cells Based on Low Bandgap Copolymer with Spin ½ Radical Additives. *Adv. Funct. Mater.* **2015**, *25* (12), 1895-1902.

(26) Zhang, Y.; Basel, T. P.; Gautam, B. R.; Yang, X.; Mascaro, D. J.; Liu, F.; Vardeny, Z. V., Spin-enhanced Organic Bulk Heterojunction Photovoltaic Solar Cells. *Nat. Commun.* **2012**, *3*, 1043.

(27) Sandén, S.; Wilson, N. M.; Wang, E.; Österbacka, R., Generation of Photoexcitations and Trap-Assisted Recombination in TQ1:PC71BM Blends. *J. Phys. Chem. C* **2017**, 121 (14), 8211-8219.

(28) Melianas, A.; Etzold, F.; Savenije, T. J.; Laquai, F.; Inganäs, O.; Kemerink, M., Photo-generated Carriers Lose Energy During Extraction from Polymer-fullerene Solar Cells. *Nat. Commun.* **2015**, *6*, 8778.

(29) Bakulin, A. A.; Xia, Y.; Bakker, H. J.; Inganäs, O.; Gao, F., Morphology, Temperature, and Field Dependence of Charge Separation in High-Efficiency Solar Cells Based on Alternating Polyquinoxaline Copolymer. *J. Phys. Chem. C* **2016**, *120* (8), 4219-4226.

(30) Wang, E.; Hou, L.; Wang, Z.; Hellström, S.; Zhang, F.; Inganäs, O.; Andersson, M. R., An Easily Synthesized Blue Polymer for High-Performance Polymer Solar Cells. *Adv. Mater.* **2010**, *22* (46), 5240-5244.

(31) Bergqvist, J.; Österberg, T.; Melianas, A.; Ever Aguirre, L.; Tang, Z.; Cai, W.; Ma, Z.; Kemerink, M.; Gedefaw, D.; Andersson, M. R. et al., Asymmetric Photocurrent Extraction in Semitransparent Laminated Flexible Organic Solar Cells. *npj Flex. Electron.* **2018**, *2* (1), 4.

(32) Murthy, D. H. K.; Melianas, A.; Tang, Z.; Juška, G.; Arlauskas, K.; Zhang, F.; Siebbeles, L. D. A.; Inganäs, O.; Savenije, T. J., Origin of Reduced Bimolecular Recombination in Blends of Conjugated Polymers and Fullerenes. *Adv. Funct. Mater.* **2013,** *23* (34), 4262-4268.

(33) Howard, I. A.; Mauer, R.; Meister, M.; Laquai, F., Effect of Morphology on Ultrafast Free Carrier Generation in Polythiophene:Fullerene Organic Solar Cells. *J. Am. Chem. Soc.* **2010,** *132* (42), 14866-14876.

(34) Isakova, A.; Karuthedath, S.; Arnold, T.; Howse, J. R.; Topham, P. D.; Toolan, D. T. W.; Laquai, F.; Lüer, L., Efficient Long-Range Electron Transfer Processes in Polyfluorene–Perylene Diimide Blends. *Nanoscale* **2018,** *10* (23), 10934-10944.

(35) Karuthedath, S.; Melianas, A.; Kan, Z.; Pranculis, V.; Wohlfahrt, M.; Khan, J. I.; Gorenflot, J.; Xia, Y.; Inganas, O.; Gulbinas, V. et al., Thermal Annealing Reduces Geminate Recombination in TQ1:N2200 All-Polymer Solar Cells. *J. Mater. Chem. A* **2018**, 6, 7428-7438.

(36) de Juan, A.; Jaumot, J.; Tauler, R., Multivariate Curve Resolution (MCR). Solving the Mixture Analysis Problem. *Anal. Meth.* **2014**, *6* (14), 4964-4976.

(37) Jaumot, J.; Gargallo, R.; de Juan, A.; Tauler, R., A Graphical User-friendly Interface for MCR-ALS: A New Tool for Multivariate Curve Resolution in MATLAB. *Chemometr. Intell. Lab.* **2005**, *76* (1), 101-110.

(38) Tauler, R., Application of Non-linear Optimization Methods to the Estimation of Multivariate Curve Resolution Solutions and of Their Feasible Band Boundaries in the Investigation of Two Chemical and Environmental Simulated Data Sets. *Anal. Chim. Acta* **2007**, *595* (1), 289-298.

(39) Tauler, R.; Smilde, A.; Kowalski, B., Selectivity, Local Rank, Three-way Data Analysis and Ambiguity in Multivariate Curve Resolution. *J. Chemometr.* **1995**, *9* (1), 31-58.

(40) Jaumot, J.; Aviñó, A.; Eritja, R.; Tauler, R.; Gargallo, R., Resolution of Parallel and Antiparallel Oligonucleotide Triple Helices Formation and Melting Processes by Multivariate Curve Resolution. *J. Biomol. Struct. Dyn.* **2003**, *21* (2), 267-278.

(41) Garrido, M.; Rius, F. X.; Larrechi, M. S., Multivariate Curve Resolution–Alternating Least Squares (MCR-ALS) Applied to Spectroscopic Data from Monitoring Chemical Reactions Processes. *Anal. Bioanal. Chem.* **2008**, *390* (8), 2059-2066.

(42) Dyer-Smith, C.; Howard, I. A.; Cabanetos, C.; El Labban, A.; Beaujuge, P. M.; Laquai, F., Interplay Between Side Chain Pattern, Polymer Aggregation, and Charge Carrier Dynamics in PBDTTPD:PCBM Bulk-Heterojunction Solar Cells. *Adv. Energy Mater.* **2015**, *5* (9), 1401778.

(43) Deshmukh, K. D.; Prasad, S. K. K.; Chandrasekaran, N.; Liu, A. C. Y.; Gann, E.; Thomsen, L.; Kabra, D.; Hodgkiss, J. M.; McNeill, C. R., Critical Role of Pendant Group Substitution on the Performance of Efficient All-Polymer Solar Cells. *Chem. Mater.* **2017**, *29* (2), 804-816.

(44) Lakhwani, G.; Rao, A.; Friend, R. H., Bimolecular Recombination in Organic Photovoltaics. *Annu. Rev. Phys. Chem.* **2014**, *65* (1), 557-581.

(45) Menke, S. M.; Sadhanala, A.; Nikolka, M.; Ran, N. A.; Ravva, M. K.; Abdel-Azeim, S.; Stern, H. L.; Wang, M.; Sirringhaus, H.; Nguyen, T.-Q. et al., Limits for Recombination in a Low Energy Loss Organic Heterojunction. *ACS Nano* **2016**, *10* (12), 10736-10744.

(46) Andersson, L. M.; Melianas, A.; Infahasaeng, Y.; Tang, Z.; Yartsev, A.; Inganäs, O.; Sundström, V., Unified Study of Recombination in Polymer:Fullerene Solar Cells Using Transient Absorption and Charge-Extraction Measurements. *J. Phys. Chem. Lett.* **2013**, *4* (12), 2069-2072.

(47) Karuthedath, S.; Firdaus, Y.; Liang, R.-Z.; Gorenflot, J.; Beaujuge, P. M.; Anthopoulos, T. D.; Laquai, F., Impact of Fullerene on the Photophysics of Ternary Small Molecule Organic Solar Cells. *Adv. Energy Mater.* **2019**, *9* (33), 1901443.

(48) Würfel, U.; Unmüssig, M., Apparent Field-Dependence of the Charge Carrier Generation in Organic Solar Cells as a Result of (Bimolecular) Recombination. *Solar RRL* **2018**, *2* (10), 1800229.

(49) Karuthedath, S.; Sauermann, T.; Egelhaaf, H.-J.; Wannemacher, R.; Brabec, C. J.; Luer, L., The Effect of Oxygen Induced Degradation on Charge Carrier Dynamics in P3HT:PCBM and Si-PCPDTBT:PCBM Thin Films and Solar Cells. *J. Mater. Chem. A* **2015**, *3* (7), 3399-3408.

(50) Xia, Y.; Musumeci, C.; Bergqvist, J.; Ma, W.; Gao, F.; Tang, Z.; Bai, S.; Jin, Y.; Zhu, C.; Kroon, R. et al., Inverted All-polymer Solar Cells Based on a Quinoxaline–Thiophene/Naphthalene-Diimide Polymer Blend Improved by Annealing. *J. Mater. Chem. A* **2016**, *4* (10), 3835-3843.

(51) Tang, M.-C.; Leung, M.-Y.; Lai, S.-L.; Ng, M.; Chan, M.-Y.; Wing-Wah Yam, V., Realization of Thermally Stimulated Delayed Phosphorescence in Arylgold(III) Complexes and Efficient Gold(III) Based Blue-Emitting Organic Light-Emitting Devices. *J. Am. Chem. Soc.* **2018**, *140* (40), 13115-13124.

(52) Leitl, M. J.; Krylova, V. A.; Djurovich, P. I.; Thompson, M. E.; Yersin, H., Phosphorescence versus Thermally Activated Delayed Fluorescence. Controlling Singlet–Triplet Splitting in Brightly Emitting and Sublimable Cu(I) Compounds. *J. Am. Chem. Soc.* **2014**, *136* (45), 16032-16038.

(53) van Reenen, S.; Kersten, S. P.; Wouters, S. H. W.; Cox, M.; Janssen, P.; Koopmans, B.; Bobbert, P. A.; Kemerink, M., Large Magnetic Field Effects in Electrochemically Doped Organic Light-emitting Diodes. *Phys. Rev. B* **2013**, *88* (12), 125203.

(54) Tang, Z.; George, Z.; Ma, Z.; Bergqvist, J.; Tvingstedt, K.; Vandewal, K.; Wang, E.; Andersson, L. M.; Andersson, M. R.; Zhang, F. et al., Semi-Transparent Tandem Organic Solar Cells with 90% Internal Quantum Efficiency. *Adv. Energy Mater.* **2012,** *2* (12), 1467-1476.

(55) Ohkita, H.; Cook, S.; Astuti, Y.; Duffy, W.; Tierney, S.; Zhang, W.; Heeney, M.; McCulloch, I.; Nelson, J.; Bradley, D. D. C.; et al., Charge Carrier Formation in Polythiophene/Fullerene Blend Films Studied by Transient Absorption Spectroscopy. *J. Am. Chem. Soc.* **2008,** *130* (10), 3030-3042.